Hartman–Perdok analysis of crystal morphology and interface topology of β-$LiNaSO_4$

Carlos M. Pina[a], Cornelis F. Woensdregt[b,*]

[a] *Institut für Mineralogie, Universität Münster, Corrensstrasse 24, D-48149 Münster, Germany*
[b] *Faculty of Earth Sciences, Utrecht University, P.O. Box 80.021, 3508 TA Utrecht, The Netherlands*

Abstract

The trigonal β-$LiNaSO_4$ low temperature polymorph belongs to the family of double sulphates with general formula $LiMSO_4$ (M = Na, NH_4, Rb, ...), which have very specific electrical properties. In this paper we present the β-$LiNaSO_4$ theoretical growth morphology based on the Hartman–Perdok theory. Therefore, Periodic Bond Chains (PBCs) have been identified in order to determine the influence of the crystal structure on the crystal morphology. The shortest PBC is parallel to $\langle 1\,0\,0 \rangle$ and consists of a one-step proto-PBC with sulphate(I)–cation–sulphate(I, 1 0 0) strong bonds. All the other PBCs are built up from strong bonds in two or more consecutive steps, e.g., sulphate (I)–cation–sulphate(II)–cation–sulphate (I, *u v w*). The corresponding *F* forms are in order of decreasing d_{hkl}: $\{1\,0\,\bar{1}\,0\}$, $\{1\,0\,\bar{1}\,1\}$, $\{0\,0\,0\,2\}$, $\{1\,0\,\bar{1}\,2\}$, $\{1\,1\,\bar{2}\,0\} = \{2\,\bar{1}\,\bar{1}\,0\}$, $\{1\,1\,\bar{2}\,2\} = \{2\,\bar{1}\,\bar{1}\,2\}$, ... For many *F* forms several different slice configurations can be defined. Attachment energies have been calculated in electrostatic point charge models with formal charges. In addition, the effect of covalent S–O bonds on the growth forms has been taken into account by decreasing the effective charge on oxygen, q_O. The theoretical growth form of β-$LiNaSO_4$ based on attachment energies calculated in the $LiNaS^{6+}O_4^{2-}$ point charge model shows the hexagonal prism $\{1\,0\,\bar{1}\,0\}$, the hexagonal pyramid $\{1\,0\,\bar{1}\,1\}$ and the pedion (0 0 0 1). When the influence of the S–O bond decreases ($LiNaS^{4+}O_4^{1.5-}$ model), the habit is slightly less elongated parallel to the *c*-axis due to the increased relative morphological importance of the pyramid form with respect to the prism. When we assume that the hexagonal prism face grows with halved slices $d_{20\bar{2}0}$ and thus using the attachment energies of $E_a^{20\bar{2}0}$ instead of those of $E_a^{10\bar{1}0}$, the growth forms changes drastically by the absence of the hexagonal prism form in both models. In addition, the trigonal prism $\{1\,1\,\bar{2}\,0\}$ is present as a minor form on this $LiNaS^{4+}O_4^{1.5-}$ model with halved $d_{20\bar{2}0}$ slices. Experimentally grown $LiNaSO_4$ crystals show habits that deviate from the theoretical growth forms. This must be due to external factors such as supersaturation and interaction of the crystal surface with the aqueous solutions during the growth. Growth experiments confirm that the growth morphology is strongly influenced by the degree of supersaturation.

Keywords: A1. Crystal morphology; A1. Surface structure; A2. Growth from solutions

*Corresponding author. Tel.: +31-30-253-5070; fax: +31-30-253-5030.
E-mail address: woens@geo.uu.nl (C.F. Woensdregt).

1. Introduction

The compound β-$LiNaSO_4$ belongs to the family of double sulphates with the general formula $LiMSO_4$ (M = Na, NH_4, Rb, ...). High and low temperature phases of these compounds with interesting electrical properties have been described elsewhere [1–3]. Measurements of some physical properties and technological applications often require special crystal shapes. Crystal morphology is controlled by both external parameters (e.g., supersaturation, temperature, impurities, etc.) and internal factors such as the crystal structure. In order to establish the influence of the latter parameter the derivation of the theoretical growth form according to the Hartman Perdok theory [4–6] is essential. Only *F* faces, of which the elementary growth layers called slices contain at least two PBCs, are important for the crystal morphology. Theoretical growth forms can be constructed by means of the so-called Wulff plots, when the central distances of *F* faces are assumed to be proportional to their attachment energies (E_a^{hkl}).

Crystals of β-$LiNaSO_4$ have been grown from an aqueous solution with equimolar cation composition by evaporation at temperatures of 50°C and 70°C. We assume that the supersaturation during the growth is higher in the solution at 70°C than at 50°C. Since the absolute orientation with respect to the crystallographic axes is unknown, the indexation of the most important trigonal prism is arbitrarily chosen as $\{1\,1\,\bar{2}\,0\}$, although it could be $\{2\,\bar{1}\,\bar{1}\,0\}$ as well. At low supersaturation (see Fig. 1a), both trigonal prisms $\{1\,1\,\bar{2}\,0\}$ and $\{2\,\bar{1}\,\bar{1}\,0\}$ are morphologically important, although the former is slightly more dominant. At higher supersaturation (Fig. 1b), this predominance of the trigonal prism $\{1\,1\,\bar{2}\,0\}$ is so strong that the habit of the crystals is trigonal prismatic instead of the ditrigonal habit at lower supersaturation. The morphological importance of the hexagonal pyramid $\{1\,0\,\bar{1}\,1\}$ and the pinacoid (0 0 0 1) is high and almost independent of the degree of supersaturation. Only one of the trigonal pyramids, $\{2\,\bar{1}\,\bar{1}\,4\}$, is important at high supersaturation. The hexagonal prism $\{1\,0\,\bar{1}\,0\}$ and the trigonal pyramid $\{1\,1\,\bar{2}\,4\}$ are always subordinate.

β-$LiNaSO_4$ has also been grown in a TMS gel [7]. At the initial stage of the crystallisation, when the supersaturation is high, the habits are dominated by one of the trigonal prisms, while at the final stage both trigonal prisms $\{1\,1\,\bar{2}\,0\}$ and $\{2\,\bar{1}\,\bar{1}\,0\}$ are present together with the hexagonal prism $\{1\,0\,\bar{1}\,0\}$. The crystals are usually terminated by a combination of $\{1\,1\,\bar{2}\,2\}$, $\{2\,\bar{1}\,\bar{1}\,2\}$, $\{1\,0\,\bar{1}\,2\}$ and occasionally (0 0 0 1).

According to the extended Bravais Friedel Donnay Harker Law of observation the larger the interplanar spacing d_{hkl} is, the more morphologically important the corresponding crystal form $\{h\,k\,l\}$ is. Taking into account the symmetry operators present in the space group P31c [8] ($\{h\,h\,2\bar{h}\,l\}$, $l = 2n$; $\{h\,k\,i\,l\}$, $h-k = 3n \rightarrow l = 2n$) the forms are in order of decreasing morphological importance with the corresponding d_{hkl} values in nm shown in parentheses: $\{1\,0\,\bar{1}\,0\}$ (0.6605 nm), $\{1\,0\,\bar{1}\,1\}$ (0.5487), $\{0\,0\,0\,2\}$ (0.4929), $\{1\,0\,\bar{1}\,2\}$ (0.3959), $\{1\,1\,\bar{2}\,0\} = \{2\,\bar{1}\,\bar{1}\,0\}$ (0.3183), $\{1\,1\,\bar{2}\,2\} = \{2\,\bar{1}\,\bar{1}\,2\}$ (0.3016), ...

The aim of this paper is to compute the theoretical growth form of β-$LiNaSO_4$ and to derive the atomic topology of the crystalline interfaces during the growth. For this purpose, *F* faces have been derived by means of the Hartman Perdok theory and attachment energies have been calculated in an electrostatic point charge model [9]. Effects of the covalency of the S O bond will be taken into account as well. The theoretical growth forms will be discussed in relation to the observed experimental growth morphologies.

2. Hartman–Perdok analysis

2.1. The crystal structure of β-$LiNaSO_4$

The β-$LiNaSO_4$ polymorph is the trigonal low temperature modification with space group P31c. Its cell parameters and atomic co-ordinates are summarised in Table 1 according to Morosin and Smith [8]. More recent refinements [10] confirm the trigonal P31c symmetry, while the atomic co-ordinates do not change substantially.

The crystal structure consists of SO_4 tetrahedra that are bonded to both Li^+ and Na^+ cations. The

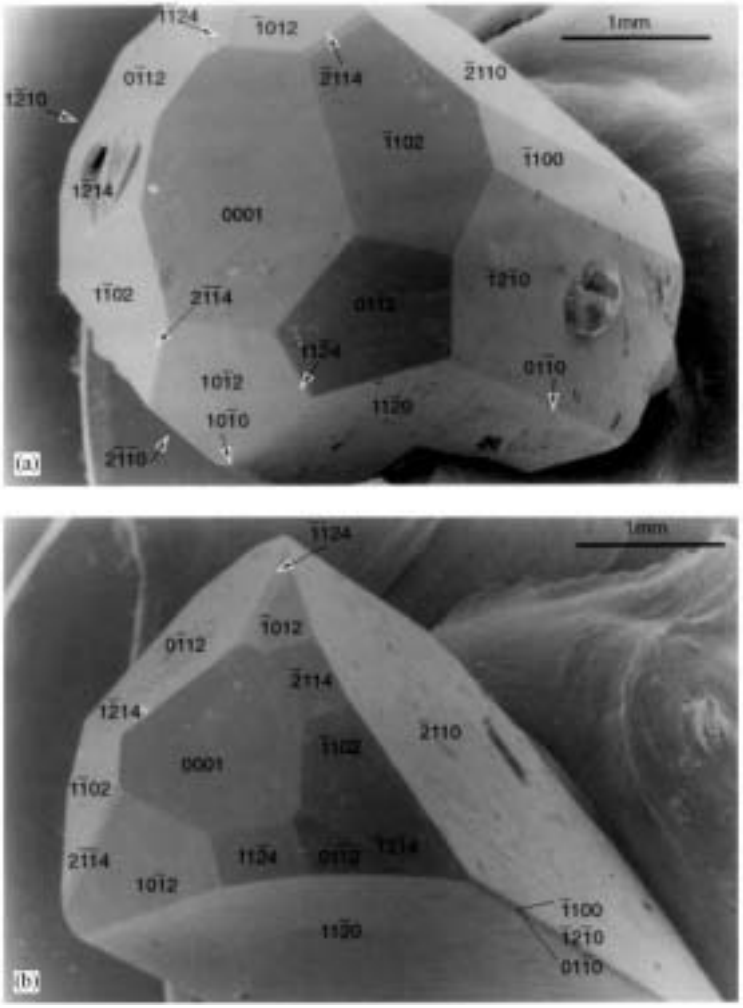

Fig. 1. β-$LiNaSO_4$ crystals grown from an aqueous solution by evaporation, (a) ditrigonal habit at 50°C, (b) trigonal habit at 70°C.

Li^+ and Na^+ ions are fourfold co-ordinated to oxygen in distorted tetrahedra and eight-fold in Archimedean antiprisms, respectively [8]. Since two of the eight bond distances are considerably larger, the eight-fold co-ordination can be questioned. For the Hartman Perdok analysis only the six-fold (octahedral) co-ordination has been considered. Since the sulphate ions are assumed to be present as one of the crystallisation units in the aqueous solution, only the bonds Li SO_4 and Na SO_4 have been taken into account as strong bonds for the qualitative PBC analysis.

For the search of PBCs we limit ourselves first to that of proto-PBCs. A proto-PBC (pPBC) is a periodic chain of strong bonds simply providing the translation along $[u\,v\,w]$ and does not necessarily comply with the condition of stoichiometry and non-polarity [1 1]. The PBC with the shortest translation period is that parallel to $\langle 1\,0\,0 \rangle$, consisting of one-step pPBCs formed by a series of consecutive sulphate (I) cation sulphate (I, 1 0 0) strong bonds. All the other proto-PBCs are built up from strong bonds in two or more consecutive steps, e.g., sulphate (I) cation sulphate (II) cation sulphate (I, $u\,v\,w$). Information

Table 1
Unit cell parameters and atomic co-ordinates of β-LiNaSO$_4$ (1) $a_0 = 0.7627$ nm and $c_0 = 0.98579$ nm[a]

Atom	x	y	z	Number (2)	
Li	0.0308	0.2503	0.2583	Li	1–6
Na	0.0252	0.5468	0.4881	Na	1–6
S(1)	0.0000	0.0000	0.0000	S	1–2
S(2)	0.3333	0.6667	0.1976	S	3–4
S(3)	0.6667	0.3333	0.2632	S	5–6
●(1)	0.0000	0.0000	0.1528	●	1–2
●(2)	0.3333	0.6667	0.3449	●	3–4
●(3)	0.6667	0.3333	0.1168	●	5–6
●(4)	0.2125	0.1108	0.9540	●	7–12
●(5)	0.2218	0.4557	0.1468	●	13–18
●(6)	0.4776	0.1697	0.3166	●	19–24

[a] (1) According to Morosin and Smith [8]. (2) Numbering in the present paper

about the specific numbering of the atoms used in this paper is given in the last column of Table 1 and can be derived from the [0 1 0] projection (Fig. 2).

In Figs. 2 and 3 only Li and Na are indicated as solid circles and numbered, while the SO_4 tetrahedra are numbered according to the central S atom. Although individual oxygens are not indicated, they are always listed in the description of the pPBCs in order to show that these PBCS comply with the conditions of a periodic bond chain, *i.e.*, not using the same identical ions twice.

2.2. The ⟨0 1 0⟩ pPBC (Fig. 2)

The strongest [0 1 0] PBC is based on periodic SO_4 (Na, Li) SO_4 chains with the shortest possible identity period of 0.7627 nm. The [0 1 0] pPBC can be described for the slice with a thickness of $d_{10\bar{1}0}$ as follows (encircled area A in Fig. 2):

S(1)−O(10)−Na(1)−O(12)−S(1, 0 1 0).

Another [0 1 0] pPBC based on the sequence: sulphate Li Li sulphate is encircled as area B in Fig. 2:

S(3)−(15)−Li(3)−O(1, 0 1 0)−Li(1, 0 1 0)
−O(13, 0 1 0)−S(3, 0 1 0).

For the *F* forms $\{h\,0\,\bar{h}\,l\}$ parallel to the [0 1 0] PBC elementary growth layers called slices can be defined. The following slices exist: for the hexagonal prism $\{1\,0\,\bar{1}\,0\}$ a slice with a thickness of $d_{10\bar{1}0}$, for the pedion (0 0 0 1) a slice with thickness of d_{0002} and for the hexagonal pyramids $\{1\,0\,\bar{1}\,1\}$ and $\{1\,0\,\bar{1}\,2\}$ slices with a thickness of $d_{10\bar{1}1}$ and $d_{10\bar{1}2}$, respectively.

2.2.1. Slice $d_{10\bar{1}0}$

Strong bonds form another pPBC, which is parallel to [0 0 1],

S(2)−O(1)−Li(1)−O(10)−S(1)−O(2)
−Li(4)−O(7)−S(2, 0 0 1) or
S(3)−O(3)−Na(1)−O(6)−S(6)−O(23)
−Na(6)−O(14, 0 0 1)−S(3, 0 0 1).

Both pPBCs connect the [0 1 0] PBC within $d_{10\bar{1}0}$, thus making $\{1\,0\,\bar{1}\,0\}$ an *F* form. This hexagonal prism is the only form present on β-LiNaSO$_4$ for which a non-polar slice configuration can be derived. This is due to the presence of *c* glide planes parallel to $\{1\,0\,\bar{1}\,0\}$ and passing through the origin and (1/2,0,0). Six different slice configurations for $\{1\,0\,\bar{1}\,0\}$ are shown in Fig. 2. Note that with the exception of $d_{10\bar{1}0_f}$ they are all nonpolar. The specific character of the $d_{10\bar{1}0_a}$ slice consists of a boundary occupied by an alternating series of one Na and one sulphate ion. The slice boundary of $d_{10\bar{1}0_b}$ is stronger undulated and occupied by the periodic sequence of sulphate Li Na. This slice boundary can be translated over half the slice thickness parallel to [1 0 0] into another slice labelled as $d_{10\bar{1}0_c}$ with a different boundary ion configuration, but with the same thickness. The $d_{10\bar{1}0_c}$ configuration is an alternating sequence of one Na and two sulphates. The slice boundaries of the pair $d_{10\bar{1}0_d}$ and $d_{10\bar{1}0_e}$ can be obtained by a

Fig. 2. In the upper left corner of the [0 1 0] projection of β-LiNaSO$_4$, Li and Na atoms are shown with their serial numbers, while these numbers for S are given in the lower right corner. Dashed lines indicate strong bonds forming pPBCs (see Section 2.2 for further explanation).

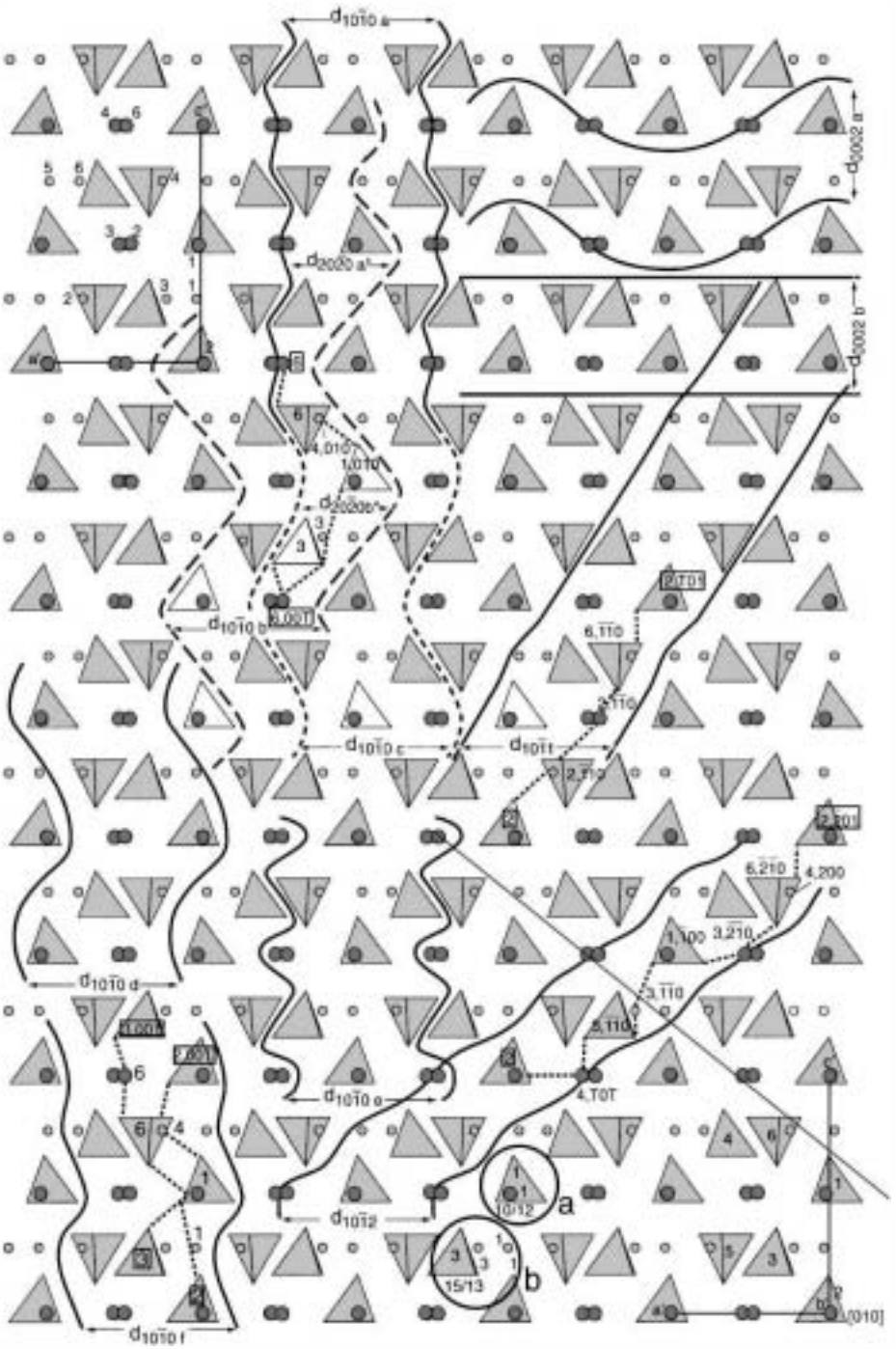
Li
Na
SO4 tetrahedron
[010]

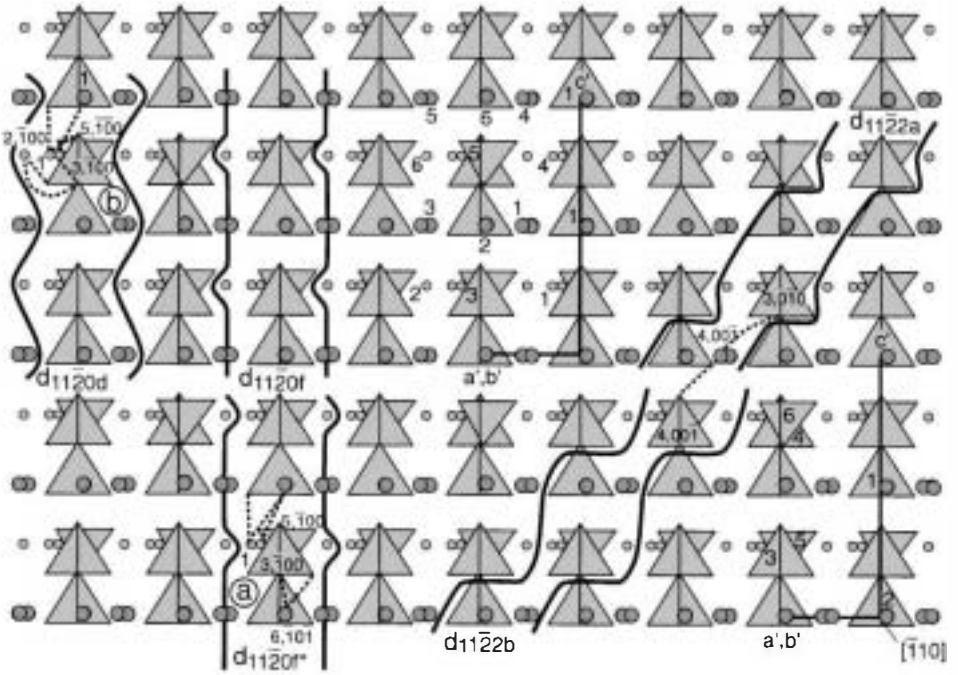

Fig. 3. In the upper central part of the [0 1 0] projection of β-LiNaSO$_4$ Li and Na atoms are shown with their serial numbers, while these numbers for S are given in the lower right corner. Dashed lines indicate strong bonds forming pPBCs (see Section 2.3 for further explanation).

translation of the $d_{1\bar{1}0_b}$ and $d_{1\bar{1}0_c}$ boundaries over 1/2 [0 0 1]. The slice configuration of $d_{1\bar{1}0_f}$ is polar, but as will be shown later, is energetically important. The halved slices $d_{2\bar{2}0}$ can be defined as slices with half the thickness of the corresponding F slice $d_{1\bar{1}0}$. An example of such a halved slice is $d_{2\bar{2}0_b}$, being the halved slice of both $d_{1\bar{1}0_b}$ and $d_{1\bar{1}0_c}$. These halved slices are genuine F slices as well, because additional pPBCs parallel to [0 0 1] can be traced within their slice boundaries. An example of such a pPBC in the case of $d_{2\bar{2}0_b}$ is as follows:

Na(6,(0 0 $\bar{1}$)−O(13/14)−S(3)−O(15)−Li(3)−O(12)
−S(1, 0 1 0)−O(2, 0 1 0)−Li(4, 0 1 0)
−O(24)−S(6)−O(23)−Na(6).

The consequences of the different surface topologies and the presence of halved slices will be discussed later.

2.2.2. *Slice* d_{0002}

According to the space group symmetry P31c, the conditions for d_{0002} must be $l = 2n$. The presence of [1 0 0] and the symmetrically equivalent [0 1 0] PBCs within this slice thickness of d_{0002} establish the F character of {0 0 0 1}. Two configurations of polar F slices are shown in Fig. 2. For the slice d_{0002_a} the surface topology consists of sulphates alternating with Na and Li ions. However, for the d_{0002_b} slice the upward oriented surface, i.e., the surface facing the positive c-axis consists of Li and sulphate ions, while Na and sulphate ions occupy the downward oriented interface, which is facing the negative c-axis. Hence, the polar character of this slice surface configuration is strongly reflected in the surface topology.

2.2.3. *Slice* $d_{1\bar{1}1}$

The [$\bar{1}$ 0 1] PBC connects the [0 1 0] PBCs within the slice with a thickness of $d_{1\bar{1}1}$. The [$\bar{1}$ 0 1] pPBC

is as follows:

S(2)−O(1)−Li(2,$\bar{1}\,\bar{1}\,0$)−O(21,$\bar{1}\,\bar{1}\,0$)−Na(2,$\bar{1}\,\bar{1}\,0$)
−O(6,$\bar{1}\,\bar{1}\,0$)−S(6,$\bar{1}\,\bar{1}\,0$)−O(24,$\bar{1}\,\bar{1}\,0$)
−Li(4,$\bar{1}\,0\,0$)−O(7,$\bar{1}\,0\,0$)−S(2,$\bar{1}\,0\,1$).

Hence $\{1\,0\,\bar{1}\,1\}$ is an F form. In Fig. 2 the energetically most favourable slice configuration is given which is bounded by an alternation of Li, Na and sulphate ions.

2.2.4. *Slice* $d_{10\bar{1}2}$

The [0 1 0] PBC is also linked to its neighbours within the slice boundaries of $d_{10\bar{1}2}$ by strong bonds parallel to [$\bar{2}$ 0 1]:

S(2)−O(8,$\bar{1}\,0\,\bar{1}$)−Na(4,$\bar{1}\,0\,\bar{1}$)−O(14,$\bar{1}\,\bar{1}\,0$)
−S(3,$\bar{1}\,\bar{1}\,0$)−O(15,$\bar{1}\,\bar{1}\,0$)−Li(3,$\bar{1}\,\bar{1}\,0$)
−O(12,$\bar{1}\,\bar{1}\,0$)−S(1,$\bar{1}\,0\,0$)−O(11,$\bar{2}\,\bar{1}\,0$)
−Na(3,$\bar{2}\,\bar{1}\,0$)−O(6,$\bar{2}\,\bar{1}\,0$)−S(6,$\bar{2}\,\bar{1}\,0$)
−O(24,$\bar{2}\,\bar{1}\,0$)−Li(4,$\bar{2}\,0\,0$)−O(7,$\bar{2}\,0\,0$)
−S(2,$\bar{2}\,0\,1$).

Hence $\{1\,0\,\bar{1}\,2\}$ has the character of an F form. Just as in the case of $d_{10\bar{1}1}$ only the most favourable slice configuration is shown in Fig. 2 with an alternating sequence of Li, Na and sulphate ions.

2.3. *The* [1 $\bar{1}$ 0] *pBC (Fig. 3)*

The [1 $\bar{1}$ 0] pPBCs are based on the six-step sequence of SO_4 (Na,Li) SO_4 (Na,Li) SO_4 [1 $\bar{1}$ 0]. Their identity periods of 1.321 nm are much larger than those of the [0 1 0] PBCs. A possible configuration of a complete [1 $\bar{1}$ 0] pPBC for the slice with a thickness of $d_{11\bar{2}0}$ is (indicated as a in Fig. 3):

S(1)−O(10)−Li(1)−O(20,$\bar{1}\,0\,0$)−S(5,$\bar{1}\,0\,0$)
−O(5,$\bar{1}\,0\,0$)−Na(6,$\bar{1}\,0\,\bar{1}$)−O(13,$\bar{1}\,0\,0$)
−S(3,$\bar{1}\,0\,0$)−O(15,$\bar{1}\,0\,0$)−Li(3,$\bar{1}\,0\,0$)
−O(12,$\bar{1}\,0\,0$)−S(1,$\bar{1}\,1\,0$).

Another possibility is that of b in Fig. 3:

S(1)−O(10)−Li(1)−O(20,$\bar{1}\,0\,0$)−S(5,$\bar{1}\,0\,0$)
−O(5,$\bar{1}\,0\,0$)−Li(2,$\bar{1}\,0\,0$)−O(14,$\bar{1}\,0\,0$)
−S(3,$\bar{1}\,0\,0$)−O(15,$\bar{1}\,0\,0$)−Li(3,$\bar{1}\,0\,0$)
−O(12,$\bar{1}\,0\,0$)−S(1,$\bar{1}\,1\,0$).

The following F forms belonging to the [$\bar{1}$ 1 0] zone are: the trigonal prism $\{1\,1\,\bar{2}\,0\}$ and the trigonal pyramid $\{1\,1\,\bar{2}\,2\}$. The crystal form $\{1\,1\,\bar{2}\,1\}$ is not an F form, because it is not possible to define a complete [$\bar{1}$ 1 0] PBC within a slice thickness of $d_{22\bar{4}2}$, which is halved due to the space group extinction rules that are for $d_{\{hh\bar{2}hl\}}$, $l = 2n$.

2.3.1. $d_{11\bar{2}0}$

The [$\bar{1}$ 1 0] PBC is connected to equivalent PBCs by strong bonds parallel to the [0 0 1] PBC within the slice thickness of $d_{11\bar{2}0}$. Consequently $\{1\,1\,\bar{2}\,0\}$ has an F character. In Fig. 3 three different slice configurations have been outlined for $\{1\,1\,\bar{2}\,0\}$. They represent the energetically most favourable slice boundaries. The surface boundary of the $d_{11\bar{2}0d}$ slice is bounded either by Li and sulphate ions or by Na and sulphate ions. The $d_{11\bar{2}0f}$ and $d_{11\bar{2}0f*}$ slice boundary configurations consist of an alternating series of Na sulphate Li sulphate ions. One of the surface boundaries of $d_{11\bar{2}0f}$ does not contain any Li boundary ions at all.

2.3.2. $d_{11\bar{2}2}$

A pPBC parallel to [$\bar{1}\,\bar{1}$ 1] connects the [$\bar{1}$ 1 0] PBCs of the b type within the slice boundaries of $d_{11\bar{2}2}$ establishing its F character. The strong bonds connecting the b type [$\bar{1}$ 1 0] PBCs are

−S(4,0 0 $\bar{1}$)−O(4,0 0 $\bar{1}$)−Na(4,0 0 $\bar{1}$)−O(15,0 $\bar{1}$ 0)
−S(3,0 $\bar{1}$ 0)−

Li and sulphate ions occupy one side of the interface, while Na and sulphate ions form the opposite interface.

2.4. *F forms*

Due to the non-centrosymmetrical trigonal structure of β-$LiNaSO_4$ crystal forms belonging to the zone of [1 2 0] are not directly equivalent to those of the [$\bar{1}$ 1 0] zone. The trigonal prism form

$\{1\,1\,\bar{2}\,0\}$ has, however, the same interplanar spacing as the other trigonal prism form $\{2\,\bar{1}\,\bar{1}\,0\}$ and thus the same slice energy. The slice energy (E_s) is the energy released per mole, when a new slice d_{hkl} is formed from the vapour neglecting the influence of edge energies. Two other pairs of forms: $\{1\,1\,\bar{2}\,1\}$–$\{2\,\bar{1}\,\bar{1}\,1\}$ and $\{1\,1\,\bar{2}\,2\}$–$\{2\,\bar{1}\,\bar{1}\,2\}$ have also the same slice thickness and slice energy. Since all these forms are polar, this means that the interface topology is not the same for both sides of each individual slice. For each pair of slices, however, the upper part of one slice is equivalent to the lower part of the other slice. The attachment energy, E_a, is defined as the energy released when a slice with a thickness of d_{hkl} crystallises on an already existing crystal face $(h\,k\,l)$. The attachment energies for $\{1\,1\,\bar{2}\,0\}$ and $\{2\,\bar{1}\,\bar{1}\,0\}$ are also identical since $E_c = E_s + E_a$, where E_c is the lattice or crystal energy. The surface structure of $\{1\,1\,\bar{2}\,0\}$ that is in contact with the medium from which it is growing is different from that of $\{2\,\bar{1}\,\bar{1}\,0\}$. This leads to different surface properties such as surface diffusion, adsorption, distribution coefficients, etc. What kind of consequences this will have on the morphology will be discussed later.

All the pPBCs found during the previous search for F slices do not produce any other F forms that have not already described. From the qualitative analysis we know now that the following forms of β-$LiNaSO_4$ are F faces: $\{1\,0\,\bar{1}\,0\}$, $\{1\,0\,\bar{1}\,1\}$, $\{0\,0\,0\,2\}$, $\{1\,0\,\bar{1}\,2\}$, $\{2\,\bar{1}\,\bar{1}\,0\}$, $\{1\,1\,\bar{2}\,0\}$, $\{1\,1\,\bar{2}\,2\}$ and $\{2\,\bar{1}\,\bar{1}\,2\}$. In the stereographic projection (Fig. 4) PBCs and resulting F forms are shown for β-$LiNaSO_4$

3. Quantitative morphology

3.1. Computation of attachment energies

Once the F faces have been identified by the qualitative PBC analysis, their relative morphological importance can be established by the order of the related attachment energies [12]. For polar slices the attachment energies cannot be calculated directly. With the exception of the hexagonal prism $\{1\,0\,\bar{1}\,0\}$, all other crystal forms $\{h\,k\,i\,l\}$ of β-$LiNaSO_4$ have only polar slices due to the absence of a symmetry centre. In all these cases the attachment energies have been derived from the relation $E_a = E_c - E_s$, where E_c is the crystal energy and E_s the slice energy [4].

Both attachment energy and slice energy calculations have been carried out in electrostatic point

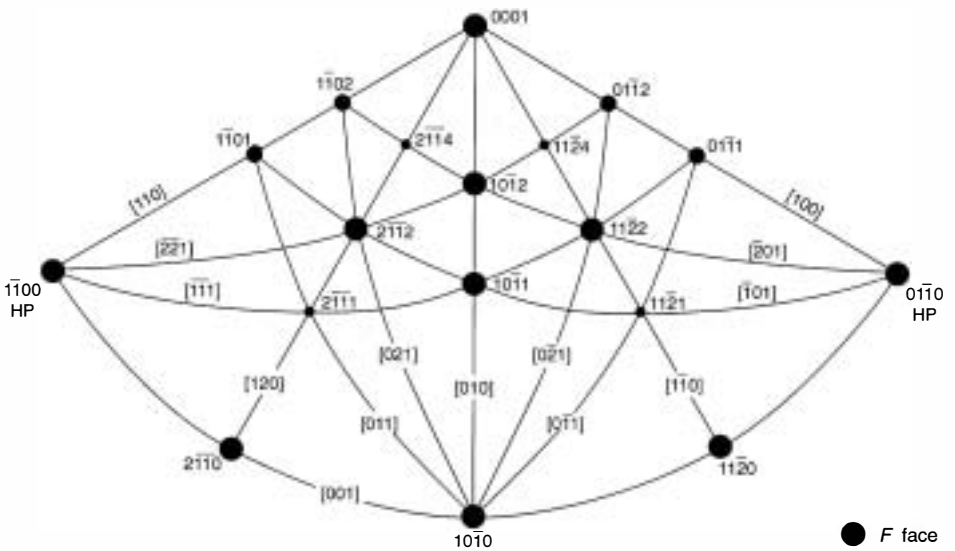

Fig. 4. In the stereographic projection of β-$LiNaSO_4$ the zone circles parallel to the PBCs are drawn as solid lines, while large solid circles indicate F faces.

charge models [9]. Formal charges have been used for Na and Li, while two different charge distribution for the sulphate ion have been used: model I: $[S^{6+}O_4^{2-}]^{2-}$ and model II: $[S^{4+}O_4^{1.5-}]^{2-}$. By decreasing the effective charges on oxygen and thus on S, the influence of the covalent character of S O bonds on the growth rates can be estimated.

The calculated attachment energies vary largely as a function of the selected slice configurations because of the large number of possible slice configurations. In this paper we present only those slice configurations with the least negative attachment energies for one particular crystal form. Configurations with much larger negative attachment energies are believed to have a lower probability of being present on the growth forms during the crystal growth process. The most relevant attachment energies computed in models I and II are summarised in Table 2.

3.2. *Hexagonal forms*

The slice $\boldsymbol{d}_{1\bar{0}10}$ exhibits many different configurations, which are always bounded by alternating Na (or Li) and SO_4 ions. The $\boldsymbol{d}_{1\bar{0}10^f}$ has the least negative attachment energy values (−219 kJ/mol in model I and −200 kJ/mol in model II) and could be considered as the most probable surface configuration. In contrast to all the other configurations, this slice configuration $\boldsymbol{d}_{1\bar{0}10^f}$ is polar. The nonpolar slices such as $\boldsymbol{d}_{1\bar{0}10^a}$ and $\boldsymbol{d}_{1\bar{0}10^d}$ represent alternatives with attachment energies, which are slightly more negative than those of $\boldsymbol{d}_{1\bar{0}10^b}$. Slices with still more negative attachment energies, such as $\boldsymbol{d}_{1\bar{0}10^b}$, $\boldsymbol{d}_{1\bar{0}10^c}$ or $\boldsymbol{d}_{1\bar{0}10^e}$, of which the slice boundaries are more undulated, are not very likely to be elementary growth layers for $\{10\bar{1}0\}$.

Each nonpolar $\boldsymbol{d}_{1\bar{0}10}$ can be divided into two symmetrically equivalent halved slices $\boldsymbol{d}_{20\bar{2}0}$ both having an F character and the same attachment energy. This halving of the slices could change the growth behaviour of the hexagonal prism face considerably. When halved slices have also an F character the growth can occur by elementary growth layers with a thickness of $\boldsymbol{d}_{2h2k2l}$ [13,14]. In case of the slices $\boldsymbol{d}_{1\bar{0}10}$ the halved slices are always polar. Halved slices have lower negative attachment energies than the complete slices. The least negative attachment energy for a $\boldsymbol{d}_{20\bar{2}0}$ slice corresponds to the configuration of $\boldsymbol{d}_{20\bar{2}0^a}$ ($E_a^{20\bar{2}0^a} = -533$ kJ/mol in model I and −482 kJ/mol in model II). Since the growth rate is proportional to the attachment energy the growth rate is at the minimum proportional to $E_a^{1\bar{0}10}$ and at the maximum to $E_a^{20\bar{2}0^a}$. In both models the attachment energy of $\boldsymbol{d}_{1\bar{0}11}$ is always about thirty percent less negative than the corresponding attachment energies of $\boldsymbol{d}_{1\bar{0}12}$.

Table 2
Attachment energies in kJ/mol of the most important F configurations of β-$LiNaSO_4$

d_{hkl} in nm	$\{hkil\}$	Attachment energies in kJ/mol	
		$q_O = -2.0\|e\|$ $q_S = +6.0\|e\|$	$q_O = -1.5\|e\|$ $q_S = +4.0\|e\|$
0.6605	$\{10\bar{1}0\}$a	−251	−226
	$\{10\bar{1}0\}$b	−303	−263
	$\{10\bar{1}0\}$c	−289	−258
	$\{10\bar{1}0\}$d	−256	−226
	$\{10\bar{1}0\}$e	−368	−342
	$\{10\bar{1}0\}$f	−219	−200
0.5487	$\{10\bar{1}1\}$b	−236	−216
0.4929	(0002) a	−302	−287
	(0002) b	−181	−193
0.3959	$\{10\bar{1}2\}$a	−314	−299
0.3183	$\{11\bar{2}0\}$d	−301	−269
	$\{11\bar{2}0\}$f	−521	−492
	$\{11\bar{2}0\}$f*	−533	−485
0.3303	$\{20\bar{2}0\}$a	−533	−482
	$\{20\bar{2}0\}$b	−630	−556
0.3016	$\{11\bar{2}2\}$b	−477	−449

3.3. *Trigonal forms*

The trigonal prisms $\{11\bar{2}0\}$ and $\{2\bar{1}\bar{1}0\}$ also show a large number of F slice configurations of which only those with the least negative attachment energy are listed in Table 2. The slice $\boldsymbol{d}_{11\bar{2}0^d}$ has the least negative attachment energy, −301 kJ/mol (model I) or 269 kJ/mol (model II), which are

of the same order as those for the hexagonal prism forms. Small changes in the surface topology produce sometimes much lower negative attachment energies. This is demonstrated for $d_{11\bar{2}0f}$, when the Na ions are selected in a different way.

Two different trigonal pyramids have been distinguished as *F* forms: $\{2\,\bar{1}\,\bar{1}\,2\}$ and $\{1\,1\,\bar{2}\,2\}$. They have a relatively large negative attachment energy compared to those of the hexagonal pyramids.

3.4. Pedion (0 0 0 1)

The attachment energy of the more undulated surface of d_{0002a} is much lower (–302 kJ/mol in model I or –287 kJ/mol in model II) than that of the flat surface of d_{0002b} (–182 kJ/mol and –193 kJ/mol, in models I and II, respectively).

3.5. Theoretical growth forms

The calculated attachment energies have been applied in a three-dimensional Wulff plot in order to visualise the theoretical growth forms. The thus obtained theoretical growth forms for the different models are presented in Fig. 5. These forms are constructed taking into account only the influence of crystal structure on the growth rates. Neither the effect of supersaturation nor the influence of impurities and Born repulsion is considered.

Fig. 5 shows the theoretical growth forms as a function of (1) halving of $d_{10\bar{1}0}$ (first and second rows) and (2) the effective charges of oxygen (left

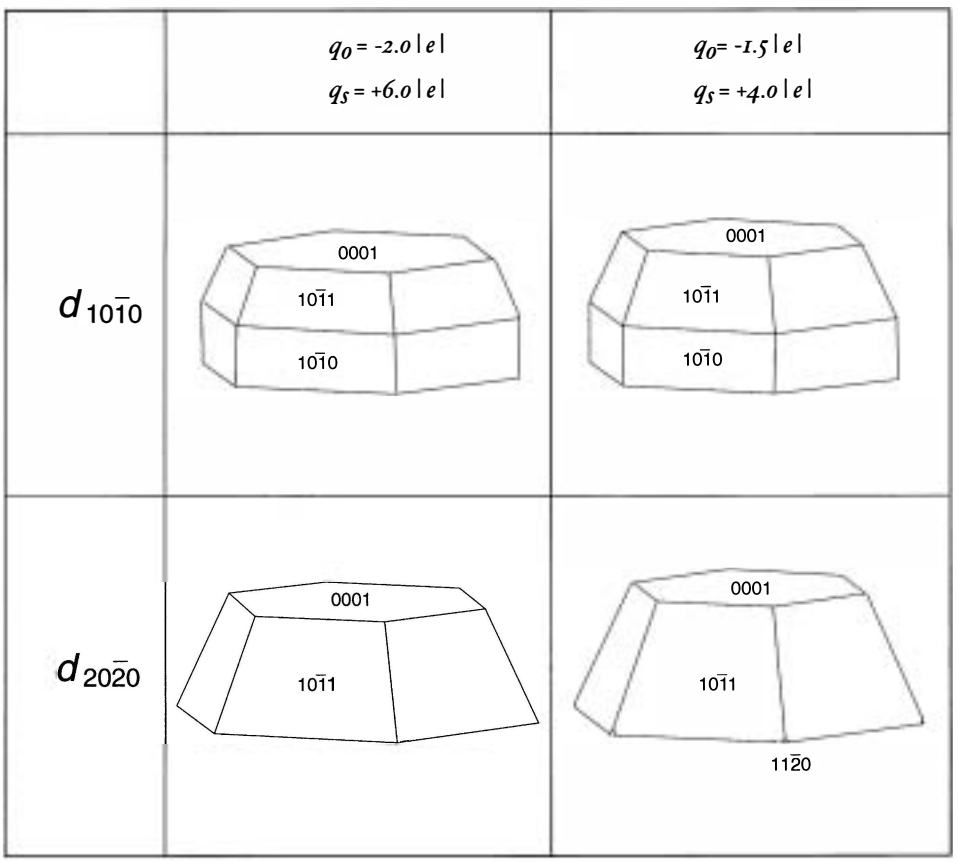

Fig. 5. Theoretical growth forms of β-$LiNaSO_4$. All forms have been constructed with equal volume by means of the CRYSTALDRAW program (see foot note 1).

and right columns, models I and II). All theoretical growth forms are constructed with the same volume and setting the $E_a^{000\bar{1}}$ at the fictive value of -0.1 kJ/mol. We have selected always the least negative E_a^{hkl} in case that for more than one slice configuration these energies have been computed.

By means of the PC-DOS CRYSDRAW program,[1] theoretical growth forms have been constructed with equal volume. Only the forms $\{h\,k\,i\,l\}$ are shown with $l \geqslant 0$ due to the absence of a symmetry centre. The theoretical growth form of β-$LiNaSO_4$ based on attachment energies calculated in the $LiNaS^{6+}O_4^{2-}$ point charge model shows the hexagonal prism $\{1\,0\,\bar{1}\,0\}$, the hexagonal pyramid $\{1\,0\,\bar{1}\,1\}$ and the pedion $(0\,0\,0\,1)$. When the influence of the S O bond decreases (model II), the habit slightly changes by an increase of the morphological importance of the pyramid form and a decrease of that of the prism. When we assume that the hexagonal prism face grows with halved slices $d_{2\bar{0}\bar{2}0}$ and thus use the attachment energies of $E_a^{20\bar{2}0}$ instead of those of $E_a^{10\bar{1}0}$, the growth forms change drastically by the absence of the hexagonal prism form in both models. In addition, the trigonal prism $\{1\,1\,\bar{2}\,0\}$ is present as a minor form in the $LiNaS^{4+}O_4^{1.5-}$ (model II) with halved $d_{2\bar{0}\bar{2}0}$ slices.

The general tendency is that crystals are slightly less elongated parallel to the c-axis, when q_0 decreases. The $E_a^{0002} : E_a^{10\bar{1}0}$ varies from 0.83 for the model with the formal charges till 0.96 for the model with the reduced charges.

Although the relative importance of the prismatic faces is determined by the halving of $d_{10\bar{1}0}$, it is not possible by means of attachment energy criterion to know how elongated the prism is. This fact is a consequence of the non-centrosymmetric structure of β-$LiNaSO_4$ and will be discussed in the next section.

4. Discussion and conclusions

All crystal faces observed on experimental growth forms are F faces according to the Hartman Perdok analysis with the exception of the trigonal pyramids $\{2\,\bar{1}\,\bar{1}\,4\}$ and $\{1\,1\,\bar{2}\,4\}$ that are S forms. In our models we cannot differentiate between the different trigonal pyramids and prisms that have the same slice thickness and thus the same attachment energy. On the gel grown crystals, trigonal prisms prevail at the first stages of the crystallisation, whereas hexagonal prismatic forms become more important when supersaturation decreases [7,15]. Similarly, the results of our growth experiments from solution indicate a correlation between the development of trigonal forms and supersaturation. The theoretical growth forms derived from the calculations of attachment energies in an electrostatic point charge model show the same morphological development of the terminal forms such as the pedion $(0\,0\,0\,1)$ and the hexagonal pyramid $\{1\,0\,\bar{1}\,1\}$. However, the (di)trigonal prismatic development of the experimental forms instead of the calculated predominance of the hexagonal prismatic form is quite different. This must be due to the difference in surface properties between the hexagonal and the trigonal prisms. The trigonal prism slices are polar and thus the effect of supersaturation on relative growth rates will be more extreme. The theoretical growth form displays only the trigonal prism as a minor form, when the effect of the S O covalent bonds (lower effective q_0) is taken into account. Hence, small variations in the relative growth rates of the trigonal and hexagonal prisms control the appearance of these prism forms.

The morphological importance of the F face $(0\,0\,0\,1)$ on the theoretical growth form is controlled by the selection of the appropriate attachment energy value. In our growth forms shown in Fig. 5 we have used the minimum value of -181 kJ/mol (model I) or -193 kJ/mol (model II). Possibly, the slice configuration of $(0\,0\,0\,2)_a$, which has a more symmetrical distribution of the Li and Na ions than the flat surface of $(0\,0\,0\,2)_b$, is more realistic. In that case, the growth forms would be much more elongated parallel to the c-axis. This prismatic habit is normally observed for the experimental crystals. However, the degree of elongation of the β-$LiNaSO_4$ cannot be predicted only by attachment energy calculations

[1] CRYSTALDRAW, PC-DOS program written by Joachim Bohm.

and must be interpreted as an effect of the external conditions on the crystal morphology.

The morphological importance of both trigonal pyramids, $\{1\,1\,\bar{2}\,2\}$ and $\{2\,\bar{1}\,\bar{1}\,2\}$ cannot be explained directly by their attachment energy values. They are both polar and have not been observed on our crystals grown from the solution by evaporation. In fact, S forms such as $\{2\,\bar{1}\,\bar{1}\,4\}$ and $\{1\,1\,\bar{2}\,4\}$ are even more important morphologically. Therefore, other external factors, such as supersaturation and the interaction of the aqueous solution with crystal surfaces, must have caused the (di)trigonal habit. Moreover, we have also observed that during the experimental growth, when the supersaturation is decreasing, sometimes the hexagonal prisms are also appearing.

The surface configurations show a large variety of boundary ions. Sometimes, only Li and sulphate or Na and sulphate are the boundary ions. The interaction of the crystalline interface with the solution will strongly depend on the surface configuration. Since no information is available from the experimental conditions, it is impossible to correlate the theoretically derived surfaces with the experimentally active surfaces.

All crystals grown experimentally are twinned more or less parallel to (0001). This can be explained by the fact that during the nucleation stage the differences in the $\{hkil\}$ and $\{\bar{h}\bar{k}\bar{i}\bar{l}\}$ surface energies are rather small. For that reason the twinning is caused by the absence of the symmetry centre in the space group P31c.

The Hartman Perdok analysis of β-$LiNaSO_4$ has shown the influence of the crystal structure on the crystal morphology. The lack of similarity between the (di)trigonal prismatic development of the experimental crystals and the hexagonal prismatic habit of the calculated growth forms demonstrates once again that the experimental morphology can also strongly be controlled by external factors. The theoretical growth morphology must be considered as an idealised reference form, which can be useful for the interpretation of experimental crystal habits obtained at different growth conditions.

Acknowledgements

The authors gratefully acknowledge Mr. H.D. Meeldijk for growing the crystals as shown in Fig. 1, measuring the spherical coordinates of their crystal faces and making the Scanning Electron Microscope images. This paper is a contribution to INTAS project 99-00247.

References

[1] S.R. Sahaya Prabaharan, P. Muthusubramanian, M. Anbu Kulandainathan, V. Kapali, J. Solid State Chem. 106 (1993) 219.

[2] D. Teeters, R. Freech, Solid State Ion. 5 (1981) 437.

[3] M.E. Kassem, M.A. El-Kolaly, K.Z. Ismail, Mater. Lett. 16 (1993) 102.

[4] P. Hartman, in: P. Hartman (Ed.), Crystal Growth: an Introduction, North-Holland, Amsterdam, 1973, pp. 367 (Chapter 14).

[5] P. Hartman, in: I. Sunagawa (Ed.), Morphology of Crystals, Part A, Terra Scientific, Tokyo and Reidel, Dordrecht, pp. 269, 1988 (Chapter 4).

[6] C.F. Woensdregt, Faraday Discuss. 95 (1993) 97.

[7] C.M. Pina, L. Fernández-Díaz, J. López-García, M. Prieto, J. Crystal Growth 148 (1995) 283.

[8] B. Morosin, D.L. Smith, Acta Crystallogr. 22 (1967) 906.

[9] C.F. Woensdregt, Phys. Chem. Miner. 19 (1992) 52.

[10] B. Granéli, P. Fischer, J. Roos, D. Brinkmann, A.W. Hewat, Physica B 180 & 181 (1992) 612.

[11] C.F. Woensdregt, H.W.M. Janssen, A. Gloubokov, A. Pajaczkowska, J. Crystal Growth 171 (1997) 392.

[12] P. Hartman, P. Bennema, J. Crystal Growth 49 (1980) 166.

[13] P. Hartman, W.M.M. Heijnen, J. Crystal Growth 63 (1983) 261.

[14] W.M.M. Heijnen, Geol. Ultraiectina, 42 (1986) 11, Ph.D. Thesis, Utrecht.

[15] C.M. Pina, Trayectorias de cristalización a partir de soluciones multicomponentes: formación de sales dobles en sistemas ternarios M_2SO_4–Li_2SO_4–H_2O (M = Na, NH_4, Rb), Complutense, 1996 (in Spanish).